Title
Local control of intracellular microtubule dynamics by EB1 photodissociation.

Journal
Nature cell biology, 20(3)

ISSN
1465-7392

Authors
van Haren, Jeffrey
Charafeddine, Rabab A
Ettinger, Andreas
et al.

Publication Date
2018-03-01

DOI
10.1038/s41556-017-0028-5

Peer reviewed

Published in final edited form as:

Nat Cell Biol. 2018 March ; 20(3): 252–261. doi:10.1038/s41556-017-0028-5.

Local Control of Intracellular Microtubule Dynamics by EB1 Photo-Dissociation

Jeffrey van Haren[1], **Rabab A. Charafeddine**[1], **Andreas Ettinger**[1,2], **Hui Wang**[3], **Klaus M. Hahn**[3], and **Torsten Wittmann**[1,4]

[1]University of California San Francisco, 513 Parnassus Avenue, San Francisco, CA 94143, U.S.A

[3]University of North Carolina Chapel Hill, Chapel Hill, NC 27599, U.S.A

Abstract

End-binding proteins, EBs, are adaptors that recruit functionally diverse +TIP proteins to growing microtubule plus ends. To test with high spatial and temporal accuracy how, when and where +TIP protein complexes contribute to dynamic cell biology, we developed a photo-inactivated EB1 variant (π-EB1) by inserting a blue light-sensitive protein-protein interaction module between the microtubule- and +TIP-binding domains of EB1. π-EB1 replaces endogenous EB1 function in the absence of blue light. In contrast, blue light-mediated π-EB1 photo-dissociation results in rapid +TIP complex disassembly, and acutely and reversibly attenuates microtubule growth independent of microtubule end association of the microtubule polymerase CKAP5 (ch-TOG, XMAP215). Local π-EB1 photo-dissociation allows subcellular microtubule dynamics control at the second and micrometre scale, and elicits aversive turning of migrating cancer cells. Importantly, light-mediated domain splitting can serve as template to optically control other intracellular protein activities.

INTRODUCTION

Microtubules (MTs) self-organize to form polarized arrays of dynamic intracellular tracks enabling directional transport, chromosome segregation and cell polarity. MT network remodeling through stochastic switching of dynamic MT plus ends between phases of growth and shortening and selective stabilization is critical for all MT functions in cells. Despite extensive biochemical insights from *in vitro* experiments and computational models[1], how MT dynamics are locally controlled inside cells and how local control contributes to complex cell and tissue morphogenesis remains unclear, and represents a

[4]Corresponding author: torsten.wittmann@ucsf.edu.
[2]Current address: Institute of Epigenetics and Stem Cells, Helmholtz Center Munich, Marchioninistrasse 25, 81377 München, Germany

AUTHOR CONTRIBUTIONS:

J.v.H. and T.W. designed the experiments, analysed the data and wrote the manuscript. J.v.H. performed most of the experiments and generated most of the reagents. A.E. and R.A.C. contributed to reagent generation and experimental work. H.W. and K.M.H. contributed unpublished reagents.

COMPETING FINANCIAL INTERESTS

The authors declare no competing financial interests.

significant gap in our understanding of physiological MT function. Interactions of growing MT plus ends with other intracellular components are mediated by a class of proteins referred to as +TIPs[2,3]. Association of most if not all +TIPs with growing MT ends requires end-binding proteins (EBs), in particular EB1 (MAPRE1) and EB3 (MAPRE3) in mammalian cells. While EBs associate with all growing MT ends, the composition of the EB-recruited +TIP complex is tightly controlled in cells in space and time[4–9]. In addition, different +TIP complexes can have antagonistic effects. EBs can recruit enzymes to growing MT ends promoting either MT polymerization[7] or depolymerization[10], and it is not known how these opposing activities are balanced. Here, we developed a strategy to inactivate the +TIP adaptor EB1 by light, a stimulus that can be controlled with high spatial and temporal accuracy and is compatible with high resolution microscopy of cell dynamics. We demonstrate that photo-inactivated π-EB1 allows accurate control of intracellular MT dynamics and function allowing new experimental paradigms and serving as a proof-of-principle of a new optogenetic protein inactivation design.

RESULTS

Design of a photo-inactivated EB1

EB1 consists of two functional domains. The N-terminal CH domain recognizes growing MT ends[11,12] while the C-terminal EBH domain recruits +TIPs[13]. We predicted that controlling their connection using light would disrupt EB1-mediated +TIP interactions with growing MT ends, without interfering with EB1-binding to MTs. Unlike most other optogenetic reagents in which light induces protein-protein interactions[14], the Protein A Z-domain-derived affibody, Zdk1[15], functions the opposite way and binds the oat phototropin 1 LOV2 domain with high affinity in the dark, but dissociates in blue light (Fig. 1a). To develop a light-sensitive EB1 variant, we inserted the LOV2/Zdk1 module into the intrinsically disordered linker between the N-terminal and C-terminal EB1 domains. Because efficient EB1 plus-end-tracking requires dimerization[16,17], we further inserted a GCN4 leucine zipper between the CH and LOV2 domains to retain dimerization and plus-end-tracking of the N-terminal half by itself. We refer to these photo-inactivated π-EB1 constructs as EB1N-LOV2 and Zdk1-EB1C (Fig. 1b). GST-EB1N-LOV2 bound 6xHis-Zdk1-EB1C and precipitated both SxIP motif (CLASP2) and CAP-Gly motif ($p150_{Glued}$) containing +TIPs from cell lysates indicating that the two π-EB1 halves interact and that Zdk1-EB1C is functional in binding known classes of +TIPs (Supplementary Fig. 1a). To directly visualize π-EB1 dynamics in cells and because tagging EB1 at either the N- or C-termini interferes with EB1 function[18], we inserted an EGFP tag N-terminal to the Zdk1 peptide. To initially test the π-EB1 light response, the LOV2 domain was photoactivated by turning on the 488 nm acquisition channel, which represents saturating blue light exposure. EGFP-Zdk1-EB1C was recruited to MT ends by non-tagged EB1N-LOV2, and dissociated from MT ends in response to blue light with a half-life <200 ms (Fig. 1c, d), which is close to the diffusion-limited turnover time of EB1 molecules on MT ends[19,20]. Zdk1-EB1C remained enriched near centrosomes that contain SxIP-motif +TIPs independent of growing MT ends[21]. Because Zdk1-binding requires the LOV2 C-terminus, we further inserted mCherry between EB1N and LOV2 to verify that the π-EB1 N-terminal half remained on growing MT ends (Fig. 1e, f). These data demonstrate that both halves of π-EB1 are

recruited to MT ends efficiently in the dark, and that blue light induces rapid π-EB1 photo-dissociation.

Acute and reversible +TIP complex disruption by π-EB1 photo-dissociation

To analyse the functional consequences of π-EB1 photo-dissociation, we generated cell lines in which endogenous EB1 activity was largely replaced by π-EB1. We chose H1299 non-small lung cancer cells because they express almost no EB3[22] (Supplementary Fig 1c). We first made H1299 lines stably expressing π-EB1 constructs. Even though both π-EB1 halves were expressed from different plasmids, selecting clonal lines showing normal MT plus end association of EGFP-Zdk1-EB1C, which requires untagged EB1N-LOV2 to be present, resulted in H1299 lines with both π-EB1 halves at similar and near endogenous levels (46 +/− 17% EB1N-LOV2; 29 +/− 11% EGFP-Zdk1-EB1C compared to endogenous EB1; n = 4). Next, endogenous EB1 was depleted in π-EB1 expressing cells by lentivirus-mediated shRNA by about 90 +/− 2% (n = 3) (Fig. 1g). These cells used in subsequent experiments were viable with no obvious phenotype, indicating that π-EB1 expression rescues loss of endogenous EB1 function.

We then asked how π-EB1 photo-dissociation affected the dynamics of mCherry-tagged +TIPs at growing MT ends. All +TIPs tested localized to MT plus ends in non-illuminated cells, but disappeared rapidly from MT ends during blue light exposure confirming that MT end association of MCAK, CLASP2, and SLAIN2 critically depends on interactions with the C-terminal domain of EB1 (Fig. 2a). In addition, +TIP dissociation was reversible over multiple cycles of light exposure (Fig. 2b; Supplementary Video 1) indicating that π-EB1 photo-dissociation rapidly and reversibly disrupts the MT plus end +TIP complex. +TIPs only dissociated from growing MT ends and not from other binding sites; e.g. CLASP2 remained at the Golgi apparatus[23] (Supplementary Fig. 2a), demonstrating that +TIP dissociation from MT ends is specific to the light-sensitive π-EB1 dissociation. EB3-mCherry also partially dissociated from MT ends upon π-EB1 photo-dissociation, likely reflecting heterodimerization with π-EB1 and supporting a dominant effect of π-EB1 photo-dissociation even in the presence of small amounts of endogenous EBs (Supplementary Fig. 2b)[17,24].

Subcellular spatial control of π-EB1 photo-dissociation

Because EB1 diffuses freely through the cytoplasm[20], spatial control requires rapid re-association of photo-dissociated π-EB1 molecules in the absence of blue light to prevent diffusion throughout the cell. Compared with wild-type, π-EB1 containing the LOV2(I427V) variant with faster dark state recovery[15,25] re-associated on growing MT ends approximately twice as fast (Fig. 2c). To minimize blue light-induced phototoxicity, we determined the minimum blue light dosage required for sustained π-EB1 photo-dissociation. To achieve a range of radiant exposures, we used pulse width modulation of a 470 nm LED (0.25-20 ms pulse lengths) at a fixed irradiance and a pulse frequency of 1 Hz between camera exposures (Fig. 2d). Compared with wild-type, the faster LOV2 domain required ~3 times more blue light to reach the same steady state π-EB1 photo-dissociation. Thus, faster LOV2 dark recovery comes at a cost of increased blue light dose. To test how this blue light exposure related to typical fluorescence microscopy light levels[26], we compared π-EB1

photo-dissociation with images of mEmerald-tagged tubulin at identical exposure settings (Supplementary Fig. 2c), indicating that π-EB1 photo-dissociation associated photodamage is likely small.

Next, we used a digital micromirror device (DMD) mask to test if LOV2 kinetics are sufficient for localized π-EB1 photo-dissociation. With the faster LOV2 variant, 20 ms 470 nm light pulses of <1 mJ mm^{-2} every second achieved intracellular gradients with 95% difference in π-EB1 photo-dissociation over a width of ~20 μm (Fig. 2e, f), and to reversibly switch π-EB1 photo-dissociation between different intracellular regions (Fig. 2g; Supplementary Video 2). The photo-dissociation boundary was similar to the edge steepness of the illumination pattern (Fig. 2f), which was much shallower than expected from the theoretical resolution limit. Thus, boundary steepness was mostly determined by sharpness of the illumination pattern edge, a potential technical limit, and to a lesser extent by diffusion of photo-dissociated molecules out of the blue light-exposed region. Because wild-type LOV2 achieved a boundary that was almost as steep at reduced blue light exposure, we used wild-type LOV2 π-EB1/EB1 shRNA cells for subsequent experiments.

Acute and local inhibition of MT growth and organization by π-EB1 photo-dissociation

Many EB1-recruited +TIPs influence MT polymerization dynamics[3], but it is not understood how potentially antagonistic +TIP activities are integrated and spatially controlled inside cells. Although previous EB1/3 siRNA depletion demonstrated MT dynamics defects[17,27], such experiments are confounded by indirect and adaptive mechanisms in genetically depleted cells and cannot directly address protein actions in real time. We therefore tested how π-EB1 photo-dissociation acutely altered MT dynamics and organization. As expected, the MT-binding half of π-EB1 remained on growing MT ends following π-EB1 photo-dissociation (Fig. 1e). However, after a few seconds, EB1N-mCherry-LOV2 comet length decreased (Supplementary Fig. 4d,e), indicative of a MT growth rate decrease[28]. Indeed, computational tracking of EB1N-mCherry-LOV2 revealed an overall attenuation of MT growth and a reduction in the number of growing MT ends within 30 s of blue light exposure (Fig. 3a, b; Supplementary Video 3), and the shift in the frame-to-frame growth rate distribution indicated that π-EB1 photo-dissociation predominantly affected fast growing MT ends (Fig. 3c). Importantly, these changes were reversible, and MT dynamics recovered within minutes of terminating blue light (Fig. 3b). Moreover, the fast kinetics of π-EB1 photo-dissociation allowed locally restricted inhibition of MT growth (Fig. 3d; Supplementary Video 4). Kymograph analysis indicated that polymerization of individual MT ends did not slow gradually. Instead, MTs abruptly switched to a slower growth rate or underwent a catastrophe following π-EB1 photo-dissociation (Fig. 3e). However, this response was not always immediate, and resulted in a decay of the MT population growth rate with a half-life of ~5 seconds (Fig. 3f), which is at least an order of magnitude slower than π-EB1 photo-dissociation itself (Fig. 1d). Together, these data demonstrate that the +TIP recruiting activity of EB1 is acutely required and sufficient to sustain fast and persistent MT growth in interphase cells.

We then tested if the observed MT growth inhibition was sufficient to reorganize the intracellular MT network. Although difficult to quantify precisely, the density of the

peripheral MT network dropped rapidly during, and recovered within minutes after terminating blue light exposure (Fig. 4a). A MT polymer decrease was further supported by a robust increase in cytoplasmic tubulin-mCherry fluorescence, which reached a new equilibrium in less than a minute ($t_{½}$ = ~12 s; Fig. 4b) as individual MTs depolymerized in response to π-EB1 photo-dissociation (Fig. 4c; Supplementary Video 5). Interestingly, two distinct MT populations responded differently. Many radial MTs underwent catastrophes and depolymerized within seconds of π-EB1 photo-dissociation (Fig. 4d) consistent with the observed delay in growth rate attenuation (Fig. 3f). In contrast, a population of more curvy MTs appeared more resistant to π-EB1 photo-dissociation indicating stabilization by mechanisms that no longer require a growth-promoting +TIP complex. To focus on the 'pioneer' MT population growing toward the leading edge of migrating cells[29], we expressed constitutively active Rac1(Q61L) in π-EB1 cells, which induces isotropic leading edge f-actin polymerization, and exposes fast MT growth that counter-balances retrograde f-actin flow[30]. Local π-EB1 photo-dissociation resulted in a dramatic retraction of these MTs from Rac1(Q61L)-induced lamellipodia (Fig. 4e; Supplementary Video 6), indicating that EB1-recruited +TIP complexes maintain fast 'pioneer' MT growth near a migrating cells leading edge. Importantly, by using patterned blue light exposure intracellular asymmetry of MT network organization could be generated rapidly and maintained for extended periods of time.

EB1 is not required to recruit the MT polymerase CKAP5 to MT ends

Because CKAP5 accelerates MT growth in vitro[2,31] and can bind the EB-dependent +TIP SLAIN2[7], we hypothesized that CKAP5 loss from MT ends in response to π-EB1 photo-dissociation may cause the observed MT growth inhibition. Consistent with previous reports, mKate2-tagged CKAP5 localized to dynamic dots at distal MT ends[32,33]. However, even in control cells only a subset of EB1 comets had associated dots of CKAP5-mKate2 (Fig. 5a), and CKAP5-mKate2 was often completely absent from elongated EB1 comets on fast-growing MT ends (Fig. 5b). In addition, quantitative comparison revealed no clear correlation between the amount of EB1 and CKAP5 associated with the same MT plus ends (Fig. 5c). We then tested if π-EB1 photo-dissociation altered intracellular CKAP5 dynamics, but even after 30 s of blue light exposure, when persistent MT growth has ceased, the relative brightness of CKAP5 dots did not significantly decrease (Fig. 5d-f; Supplementary Video 7).

Because we were concerned of incomplete and variable EB1 depletion by shRNA, we next deleted both the EB1 and EB3 genes in H1299 cells by CRISPR/Cas9 genome editing (Supplementary Fig. 3a). This eliminated both EB1 and potentially compensatory EB3 expression (Supplementary Fig. 3b, c) and EB-dependent +TIP recruitment (Supplementary Fig. 3d). Nevertheless, even in these genetically deleted EB1/3 −/− cells CKAP5-mKate2 still associated with growing MT ends (Supplementary Fig. 3e; Supplementary Video 8). In addition, MT growth was inhibited in EB1/3 −/− cells and indistinguishable from what we observed in blue light exposed π-EB1-expressing EB1 shRNA cells (Fig. 5g). Importantly, both in EB1 shRNA cells and in EB1/3 −/− cells only expression of both π-EB1 halves (Supplementary Fig. 4a, b) rescued MT growth rate and comet length in a light-dependent manner (Fig. 5h; Supplementary Video 9; Supplementary Fig. 4c-e), but expression of the

N-terminal MT-binding half alone, EB1N-mCherry-LOV2, did not (Fig. 5g). CKAP5-mKate2 associated with a population of growing MT ends in EB1/3 −/− π-EB1 rescue cells both in the dark and during blue light exposure (Supplementary Fig. 4f). Together these data demonstrate that CKAP5 MT plus end association is independent of EB1-mediated +TIP recruitment, and thus cannot explain MT growth inhibition by π-EB1 photo-dissociation.

Local π-EB1 photo-dissociation induces rapid cell turning

Persistent MT growth toward the leading edge has long been speculated to maintain directional cell migration[34–36]. However, due to the lack of experimental tools to manipulate intracellular MT dynamics with high spatial and temporal accuracy the central question to what extent MT network polarity is a cause or consequence of directional migration has not been adequately addressed. We therefore used our CRISPR EB1/3 −/− π-EB1 rescue cells to ask how acute interference with EB-dependent MT plus end interactions influenced directional cell migration. We focussed on randomly migrating single cells in the absence of other chemical or haptotactic cues. As expected, wild-type H1299 cells did not react to local blue light exposure (Fig. 6a). In contrast, EB1/3 −/− π-EB1 rescue cells consistently turned away from blue light exposed regions that were placed in the front half of a migrating cell (Fig. 6b). Although H1299 cells often switched direction and random protrusion dynamics contributed substantially to centroid trajectory directional noise, in a quantitative comparison of multiple cells the only significant direction change occurred as a response to local blue light exposure in EB1/3 −/− π-EB1 rescue cells (Fig. 6c). We then tested if this aversive turning response to local π-EB1 photo-dissociation was sufficient to confine a migrating cell within a predefined region. Indeed, even though these cells are highly motile, EB1/3 −/− π-EB1 rescue cells were unable to escape from a blue light box and reversed direction every time the cell touched the virtual blue light barrier for an observation period of over 8 hours (Fig. 6d; Supplementary Video 10). Thus, EB1-mediated interactions of +TIP complexes with growing MT ends are necessary to maintain leading edge identity and directionality during cell migration.

DISCUSSION

To locally dissect complex and dynamic cell biology, new methods are needed to rapidly inactivate specific protein activities inside cells. Here, we use the +TIP-recruiting activity of EB1 as a proof-of-principle to photo-inactivate specific protein functions by inserting a light-sensitive LOV2/Zdk1 protein-protein interaction module between functional domains. Unlike genetic methods that are orders of magnitude too slow to dissect highly dynamic MT and +TIP functions and offer no spatial control, we demonstrate acute reversible π-EB1 photo-dissociation and control of intracellular MT dynamics at second and micrometre accuracy inside live cells. In contrast to genetic methods to silence or knockout genes this approach allows replacement of a protein of interest with a photo-inactivated π-variant that can be fully characterized for normal function in the absence of blue light. Thus, acute and local photo-inactivation can be used to directly observe and analyse a cellular response, rather than inferring protein function from a cell population in which a gene of interest has been removed and in which cells may have adapted to the loss of function through poorly controlled compensatory mechanisms. In the case of +TIP or other complex protein

networks, biochemical competition[37] may further complicate mechanistic interpretation of depletion or knockout phenotypes. To our knowledge, this light-induced reversible domain splitting is the only optogenetic method to allow acute, reversible and specific loss-of-function experiments. Most other optogenetic tools rely on gain-of-function in which proteins are activated, relocalized or aggregated by light. There are only few methods of light-induced protein inactivation that are either slow and irreversible such as protein depletion by light-induced proteolysis[38] or genome editing[39], or require large a priori knowledge of target protein structure[40].

Acute π-EB1 photo-dissociation allowed us to obtain new insight into the role of EB1 and the associated +TIP complex in the physiological control of MT dynamics and function. Although we only tested a subset of SxIP-motif +TIPs, recruitment of all known +TIPs depends on interactions with the EB1 C-terminus[3,41]. We thus think that π-EB1 photo-dissociation results in a broad disruption of +TIP association with MT ends. *In vitro*, EB1 stimulates tubulin GTP hydrolysis and increases the catastrophe frequency[12,42,43], but only moderately increases the MT growth rate at high EB1 concentrations. In contrast, we find that in cells EB1-mediated +TIP complexes maintain fast and persistent MT growth. Thus, the EB1 intrinsic MT destabilizing activity is outweighed by the growth-promoting activity of the EB1-recruited +TIP complex. Because the N-terminal half of π-EB1 remains on growing MT ends after photo-dissociation, structural changes induced by EB1 binding[12] are insufficient to maintain persistent MT growth. In contrast to previous reports[17], at physiological expression levels, the N-terminal MT binding half of EB1 by itself had no noticeable effect on intracellular MT dynamics. The growth-promoting activity of the EB1-mediated +TIP complex also cannot easily be explained by interactions with the canonical MT polymerase CKAP5. CKAP5 association with the most distal tips of MT plus ends does not correlate well with EB1 localization and does not depend on EB1 either in π-EB1 photo-dissociation experiments or in cells in which we removed EB1 and EB3 by genome editing. While this is consistent with EB1-independent CKAP5 localization to MT ends *in vitro*[31], this was surprising as CKAP5 recruitment to growing MT ends in cells was previously attributed to EB1-mediated interactions with the +TIP SLAIN2[7,33], which rapidly disappears from growing MT ends upon π-EB1 photo-dissociation. In any case, our results show that in the absence of an EB1-recruited +TIP complex CKAP5 by itself cannot maintain physiological MT growth, and additional mechanisms that control CKAP5 activity could be involved. Strikingly, individual MTs respond to π-EB1 photo-dissociation stochastically and often continue to grow for some time before switching abruptly from fast to slow growth, indicating a sudden state change of the growing MT end seconds after +TIP complex dissociation. Thus, alternatively, the +TIP complex may stabilize the protective GTP-like MT end cap[44] in cells independent of CKAP5.

As an example to demonstrate the utility of π-EB1 in interrogating dynamic cell biology, we asked if local +TIP dissociation suffices to influence migration of cancer cells in which we replaced EB1 and EB3 with π-EB1. We find that the response of migrating H1299 small lung cancer cells to local π-EB1 photo-dissociation is remarkably robust: cells invariably turned away from the area of blue light exposure within minutes and were unable to cross a virtual blue light boundary. Thus, even in this highly transformed metastatic cancer cell line, +TIP mediated MT interactions in the cell front are essential to define and maintain

directional polarity. This is consistent with our previous finding that cell-matrix adhesion associated MT tracks support localized secretion of matrix metalloprotease activity[45], which supports a MT involvement in invasive cancer cell migration and emerging ideas that MT-directed cancer chemotherapy targets cell functions other than mitosis[46].

In summary, regardless of the precise mechanism by which EB1-recruited +TIP complexes maintain physiological MT growth rates, our data demonstrate local and acute modulation of intracellular MT dynamics with spatial and temporal accuracy that surpasses recent photopharmacological approaches[47], and together with selective optogenetic recruitment of specific proteins to MT ends[48] will allow precise dissection of +TIP functions in complex cell biology. Lastly, insertion of a light-sensitive protein-protein interaction module between functional domains is a powerful strategy applicable to a large fraction of the proteome enabling new spatially and temporally resolved experimental questions that cannot be addressed by other genetic or pharmacological means.

METHODS

DNA constructs and molecular cloning

mCherry-EB3 was from the Michael Davidson plasmid collection (Addgene plasmid #55037). mCherry-CLASP2γ was cloned by replacing the AgeI/KpnI restriction fragment of pEGFP-CLASP2γ[49] with the corresponding fragment of pmCherry-C1. Similarly, mCherry-MCAK was cloned by replacing the AgeI/BsrGI fragment of mEmerald-MCAK (Addgene plasmid #54161, from Michael Davidson) with the corresponding fragment of pmCherry-C1. mCherry-α-tubulin was obtained from Roger Tsien (Addgene plasmid #49149). PCR-based cloning strategies for other constructs are summarized below, and all primers used are listed in Supplementary Table 2:

1. EB1N-LZ-LOV2 was constructed as follows: The coding regions corresponding to amino acids 1-185 of an EB1 shRNA-resistant variant[27] and a GCN4 leucine zipper (generated by oligonucleotide assembly PCR) were first amplified, and then connected by overlap extension PCR, and the resulting product ligated into the NheI/XhoI digested backbone of pEGFP-C1. The LOV2 coding sequence originated from PA-Rac1 (Addgene plasmid #22027)[50], and L406/407A mutations that were reported to stabilize docking of the Jα-helix[51] as well as a GSGSG linker sequence were introduced by PCR. This modified LOV2 domain including the linker was amplified and inserted into the SacII/BamHI sites of the EB1N-LZ plasmid.
2. EB1N-mCherry-LOV2 was cloned by inserting PCR amplified mCherry coding sequences into XhoI/SacII sites between the LZ and LOV2 in EB1N-LZ-LOV2.
3. EB1N-EGFP-LOV2 was cloned by inserting the coding sequence for the PCR-amplified GCN4 leucine zipper into the SacII site of EB1N-EGFP-LOV2 by Gibson assembly between EGFP and LOV2.
4. mCherry-Zdk1-EB1C was cloned in the following way: PCR-amplified mCherry-Zdk1-linker (from pTriEx-mCherry-Zdk1, Addgene plasmid #81057) and the EB1 C-terminal fragment corresponding to amino acids 186-268 were

connected by overlap extension PCR. The resulting PCR product was inserted into the NheI/XhoI sites of pEGFP-C1 .EGFP-Zdk1-EB1C was generated by excising EGFP from pEGFP-C1 by restriction digestion with NheI/BsrGI and ligation into NheI/BsrGI digested mCherry-ZDK1-EB1C, thereby replacing mCherry with EGFP.

5. GST-EB1N-LZ-LOV2 was cloned by inserting PCR amplified EB1N-LZ-LOV2 into the BamHI/XmaI sites of pGEX-4T-2 (GE Life Sciences).
6. 6xHis-Zdk1-EB1C was cloned by inserting PCR-amplified ZDK1-EB1C into NheI/XhoI sites of pET28a.
7. GST-LOV2 was cloned by inserting the PCR-amplified LOV2 coding sequence including a GSGSG linker into BamHI/XhoI sites of pGEX-4T-2.
8. mCherry-Slain2 was cloned by inserting the PCR amplified SLAIN2 coding sequence into the XhoI/EcoRI sites of pBio-mCherry-C1.
9. CKAP5-mKate2 was cloned by inserting the PCR amplified mKate2 coding sequence into the BamHI/NotI sites of chTOG-GFP (Addgene #29480, from Linda Wordeman)

Cell culture and generation of π-EB1 cell lines

NCI-H1299 human non-small cell lung cancer cells were cultured in RPMI1640 supplemented with 10%FBS, penicillin/streptomycin and non-essential amino acids at 37°C, 5% CO_2 in a humidified tissue culture incubator. According to NIH guidelines, the identity of NCI-H1299 cells was confirmed by short tandem repeat profiling (IDEXX BioResearch) using a standard 9-marker panel: AMEL(X); CSF1PO(12); D13S317(12); D16S539(12,13); D5S818(11); D7S820(10); THO1(6,9.3); TPOX(8); vWA(16,17,18). The profile obtained was identical to the one reported by the ATCC.

π-EB1/EB1 shRNA cells—To replace endogenous EB1 with π-EB1 and prevent cells from adapting to EB1 depletion, we first generated stable cell lines expressing both halves of an shRNA resistant variant of π-EB1. H1299 cells were transfected with both untagged EB1N-LOV2 and EGFP-Zdk1-EB1C plasmids and selected with 500 μg/ml G418. Clones expressing both halves at comparable expression levels were identified by microscopy and colonies selected in which EGFP-Zdk1-EB1C was clearly localized to growing MT ends, which requires presence of the unlabelled N-terminal part. Colonies with low MT plus-end to cytoplasm ratio or displaying strong MT lattice labelling were discarded because expression of both halves was expected to be unequal. Expression of both π-EB1 halves was verified by immunoblot using antibodies that specifically recognize either the EB1 N- (Thermo Fisher Scientific Clone 1A11/4) or C-terminal half (BD Biosciences Clone 5/EB1). Next we knocked down endogenous EB1 in these clones by pLKO.1 lentivirus-mediated shRNA. The EB1 shRNA lentivirus and shRNA resistant variants were as described[27]. Selected colonies were sorted at the UCSF Parnassus Flow Cytometry Core to obtain a homogenous population of cells. π-EB1 cells were then transfected with mCherry-tagged constructs for functional experiments either using Fugene6 (Roche) or Lipofectamine 2000 (Life Technologies) according to manufacturer's instructions.

EB1/3 −/− π-EB1 rescue cells—EB1/EB3 double knockout cell lines were generated by CRISPR/Cas9 mediated genome editing. Cells were transfected with a mixture of pSpCas9(BB)-2A-GFP (PX458; Addgene #48138)[52] plasmids encoding three different guide RNAs targeting exons 1 of either EB1 or EB3 (gRNA sequences are included in supplementary Table 1). GFP positive cells were single cell sorted into 96-well plates and individual clones were analysed by immunofluorescence, immunoblotting and genomic PCR (supplementary Table 1). EB1/3 double knockout π-EB1 rescue cells were generated by transfection of π-EB1 constructs followed by selection as described above. Detailed methods pertaining to the generation of π-EB1 cells are made available on the Nature Protocol Exchange.[53]

EB1/3 immunofluorescence

Cells grown on clean #1.5 glass coverslips (64-0713, Warner Instruments) were fixed in -20°C methanol for 10 min, washed with PBS and blocked with blocking buffer (PBS, 2% BSA, 0.05% Tween 20) for 30 min. Mouse anti-EB1 (BD Biosciences Clone 5/EB1) and rat anti-EB3 (KT36, Absea) antibodies were diluted in blocking buffer and 50 µl drops were spotted on a sheet of parafilm in a humidified chamber. Coverslips were placed on top of these droplets (cells facing down), and incubated for one hour at room temperature, after which the coverslips were washed 3 times in PBS, 0.05% Tween 20. Fluorescent secondary antibodies (Alexa488 or Alexa568 conjugated goat anti-mouse or rat antibodies, Invitrogen) were diluted in blocking solution, and coverslips incubated and washed as above. Coverslips were dehydrated by brief immersion in 70% ethanol followed by 100% ethanol, air dried and mounted in Mowiol mounting medium (0.1 M Tris-HCl pH8.5, 25% glycerol, 10% Mowiol 4-88). Detailed information on all antibodies used in this study are included in Supplementary Table 1.

In vitro binding assays and native PAGE

GST- and 6xHis-tagged proteins were produced in *E.coli* BL21 using standard protocols. Briefly, bacteria were lysed by three freeze thaw cycles in dry-ice in lysis buffer (TBS, 0.5% TX-100, 1mM PMSF, 0.5mg/ml lysozyme) followed by DNAse treatment (1µg/ml). Lysates were cleared by centrifugation at 16000g for 10 min at 4^{o}C, and incubated with glutathione sepharose (GE Healthcare), or Talon resin (Clontech). Affinity resins were washed twice with low salt buffer (TBS, 0.1% TX-100, 5mM 2-mercaptoethanol), three times with high salt buffer (TBS, 650mM NaCl, 0.1% TX-100, 5mM 2-mercaptoethanol). For purification of LOV2-containing constructs, an additional incubation step with low salt buffer containing 5 mg/ml riboflavin 5'-phosphate (FMN) to ensure stoichiometric loading of the LOV2 domain with the FMN co-factor. Proteins were eluted in low salt buffer containing either 25 mM reduced glutathione (pH 8.5), or 150mM imidazole, dialyzed and concentrated (Amicon Ultra-15 centrifugal filters, 3000MWCO), and aliquots snap-frozen in liquid nitrogen.

Interaction between LOV2 and Zdk1 was monitored by discontinuous native PAGE. Purified LOV2 and Zdk1 fusion proteins were mixed and incubated for 30 min at 4°C, and LOV2/Zdk1 complexes run on 6% native PAGE gels in Tris-Glycine buffer pH 8.3 at 75 V for 2 hours. A custom made 470 nm LED array was placed in front of the electrophoresis tank to photoactivate LOV2 as the proteins migrated through the gel.

To test π-EB1 +TIP-binding *in vitro*, H1299 cells were lysed in ice cold 50 mM Tris-HCl, 150 mM NaCl, 0.1% Triton X-100, containing protease inhibitors (cOmplete Protease Inhibitor Cocktail, Sigma) for 30 min. Lysates were cleared by centrifugation at 13000 rpm in an Eppendorf microcentrifuge, and added to glutathione sepharose beads loaded with GST-EB1N-LZ-LOV2 and 6xHis-Zdk1-EB1C, incubated on ice for 30 min, and washed extensively. Bound proteins were analyzed by SDS-PAGE, wet transfer to nitrocellulose (GVS, 1212590) for 1 h at 60V (Bio-Rad Mini Trans-Blot), and chemiluminescent detection with horseradish peroxidase-conjugated secondary antibodies using a Fluorchem Q gel documentation system (92-14116-00, Alpha Innotech) using standard protocols. Primary antibodies: Mouse anti-$p150_{Glued}$ (BD Transduction Laboratories); rat anti CLASP2 (KT68, Absea).

Microscopy, photoactivation and image analysis—Fluorescent protein dynamics were imaged by spinning disk or TIRF microscopy on a customized microscope setup essentially as described[26,45,54], except that the system was upgraded with a next generation scientific CCD camera (cMyo, Photometrics) with 4.5 μm pixels allowing optimal spatial sampling using a 60x NA 1.49 objective (CFI APO TIRF; Nikon). Global π-EB1 photo-dissociation was achieved by turning on the 488 nm excitation channel. An irradiance of ~250 mW/cm^2 was sufficient to photoactivate the LOV2 domain although simultaneous imaging of EGFP-tagged proteins required higher light intensity. Irradiance at the specimen plane was measured using a X-Cite XR2100 light power meter (EXFO Photonic Solutions).

To achieve subcellular π-EB1 photo-dissociation, a digital micromirror device (Polygon 400, Mightex) equipped with a 470 nm LED was mounted on a Nikon TI auxiliary camera port equipped with a beamsplitter such that 20% of the light path was diverted for photoactivation and 80% was used for spinning disk confocal microscopy. This also allowed for direct imaging of the reflected illumination pattern to accurately focus and align the Polygon 400 as well as simultaneous imaging and π-EB1 photo-dissociation. To eliminate scattered photoactivation light in the imaging channel, the Polygon 400 was operated such that short 10-20 ms blue light pulses were triggered to occur between image acquisitions. For fast time-lapse experiments (at or above 1 frame per second), the Polygon 400 was directly triggered by the camera using a short delay of a few hundred ms after camera exposure. For slower time-lapse experiments, the camera trigger was used to start a pre-programmed pulse sequence between exposures using an ASI MS2000 Sequencer module.

Image analysis was performed in NIS Elements 4.3 or Fiji[55]. Fluorescence intensities were measured in small regions of 3-5 pixel diameter on MT ends that were moved in time with MT growth, and nearby cytoplasm as local background. MT end/cytoplasm ratios were calculated as previously described[56]. A ratio of one indicates no measurable difference between MT end and local cytoplasm. MT plus end tracking of mCherry-EB1N was done using u-track version 2.1.3[57,58]. 'Comet Detection' parameters were adapted to decrease the number of false positive detections as follows: 'High-pass Gaussian standard deviation': 6; Watershed segmentation 'Minimum threshold': between 6 and 8; other parameters remained at default settings. Similarly, in the 'Tracking' step, the 'Minimum Length of Track Segments' was set to 4. In order to not bias average MT growth rates toward shorter tracks, frame-to-frame MT growth rates were extracted from the 'tracksFinal' structure using a

custom MatLab script, and frame-to-frame displacements of less than 0.5 pixels were excluded. Tubulin-mCherry labelled MTs ends were tracked using the Fiji MtrackJ plugin[59].

To analyse the cell migration response to π-EB1 photo-dissociation, cells were recorded at 1 frame per minute for at least 30 min to select cells that were actively migrating and determine the pre-exposure direction of migration. Blue light regions were manually drawn roughly targeting the front or side of the migrating cell, and blue light patterns were pulsed at 1 Hz frequency. The cell outline was determined by fluorescent signal threshold and the centroid position calculated in NIS Elements for each time point. To reduce positional noise of the centroid position due to transient cell shape changes and protrusive activity, the centroid position was smoothened using a 9-frame running average. The angle between 15-min linear segments along this centroid trajectory and centred on the time of π-EB1 photo-dissociation (i.e 0 min) was then calculated by linear algebra. Turning away from the light-exposed region was defined as a positive angle.

Statistics and Reproducibility

Statistical analysis was done with the Analyse-It plugin for Microsoft Excel. Statistical significance of multiple comparisons was calculated using the Tukey-Kramer HSD test after confirming normal distribution of the data by Shapiro Wilk testing. Least square curve fitting was performed using the Solver plugin in Microsoft Excel[60], and 95% confidence intervals of the fit were calculated as described[61]. Figures were assembled in Adobe Illustrator CS5, and videos using Apple QuickTime Pro. Box-and-whisker plots show median, first and third quartile, observations within 1.5 times the interquartile range, and all individual data points. All experiments showing representative gel images or immunoblots (Figs. 1a, g; Supplementary Figs. 1a, b; 3a, b; 4a), or representative microscopy data (Figs. 2b, e; 3d; 4c, e; 5b, e, g, h; 6d; Supplementary Figs. 1c, 2; 3c, d, e; 4b, c, f) were repeated at least 3 times with similar results.

Code Availability

The u-track particle tracking package for Matlab is available from the Danuser lab at http://www.utsouthwestern.edu/labs/danuser/software/.

Data Availability

Statistical source data for Figures 1d, f; 2a-d; 3b, c, f; 4b, d; 5c, f; 6c and supplementary Figure 4e are included in Supplementary Table 3. All other data supporting the findings of this study are available from the corresponding author on reasonable request.

Supplementary Material

Refer to Web version on PubMed Central for supplementary material.

Acknowledgments

This work was supported by National Institutes of Health grants R01 GM079139, R01 GM094819, and S10 RR26758 to T.W., and P41 EB002025 and R35 GM122596 to K.H. We thank all members of the CTB community for discussions and comments on the manuscript.

References

1. Ohi R, Zanic M. Ahead of the Curve: New Insights into Microtubule Dynamics. F1000Res. 2016; 5
2. Akhmanova A, Steinmetz MO. Control of microtubule organization and dynamics: two ends in the limelight. Nat Rev Mol Cell Biol. 2015; 16:711–726. [PubMed: 26562752]
3. Kumar P, Wittmann T. +TIPs: SxIPping along microtubule ends. Trends Cell Biol. 2012; 22:418–428. [PubMed: 22748381]
4. Kumar P, et al. GSK3beta phosphorylation modulates CLASP-microtubule association and lamella microtubule attachment. J Cell Biol. 2009; 184:895–908. [PubMed: 19289791]
5. Pemble H, Kumar P, van HJ, Wittmann T. GSK3-mediated CLASP2 phosphorylation modulates kinetochore dynamics. J Cell Sci. 2017; 130:1404–1412. [PubMed: 28232523]
6. Smyth JT, et al. Phosphoregulation of STIM1 leads to exclusion of the endoplasmic reticulum from the mitotic spindle. Curr Biol. 2012; 22:1487–1493. [PubMed: 22748319]
7. van der Vaart B, et al. SLAIN2 links microtubule plus end-tracking proteins and controls microtubule growth in interphase. J Cell Biol. 2011; 193:1083–1099. [PubMed: 21646404]
8. van Haren J, et al. Dynamic microtubules catalyze formation of navigator-TRIO complexes to regulate neurite extension. Curr Biol. 2014; 24:1778–1785. [PubMed: 25065758]
9. Wu X, et al. Skin stem cells orchestrate directional migration by regulating microtubule-ACF7 connections through GSK3beta. Cell. 2011; 144:341–352. [PubMed: 21295697]
10. Montenegro GS, et al. In vitro reconstitution of the functional interplay between MCAK and EB3 at microtubule plus ends. Curr Biol. 2010; 20:1717–1722. [PubMed: 20850319]
11. Maurer SP, et al. EBs Recognize a Nucleotide-Dependent Structural Cap at Growing Microtubule Ends. Cell. 2012; 149:371–382. [PubMed: 22500803]
12. Zhang R, Alushin GM, Brown A, Nogales E. Mechanistic Origin of Microtubule Dynamic Instability and Its Modulation by EB Proteins. Cell. 2015; 162:849–859. [PubMed: 26234155]
13. Honnappa S, et al. An EB1-binding motif acts as a microtubule tip localization signal. Cell. 2009; 138:366–376. [PubMed: 19632184]
14. Repina NA, et al. At Light Speed: Advances in Optogenetic Systems for Regulating Cell Signaling and Behavior. Annu Rev Chem Biomol Eng. 2017; 8:13–39. [PubMed: 28592174]
15. Wang H, et al. LOVTRAP: an optogenetic system for photoinduced protein dissociation. Nat Methods. 2016; 13:755–758. [PubMed: 27427858]
16. Slep KC, Vale RD. Structural basis of microtubule plus end tracking by XMAP215, CLIP-170, and EB1. Mol Cell. 2007; 27:976–991. [PubMed: 17889670]
17. Komarova Y, et al. Mammalian end binding proteins control persistent microtubule growth. J Cell Biol. 2009; 184:691–706. [PubMed: 19255245]
18. Skube SB, Chaverri JM, Goodson HV. Effect of GFP tags on the localization of EB1 and EB1 fragments in vivo. Cell Motil Cytoskeleton. 2009
19. Dragestein KA, et al. Dynamic behavior of GFP-CLIP-170 reveals fast protein turnover on microtubule plus ends. J Cell Biol. 2008; 180:729–737. [PubMed: 18283108]
20. Seetapun D, et al. Estimating the microtubule GTP cap size in vivo. Curr Biol. 2012; 22:1681–1687. [PubMed: 22902755]
21. Yan X, Habedanck R, Nigg EA. A complex of two centrosomal proteins, CAP350 and FOP, cooperates with EB1 in microtubule anchoring. Mol Biol Cell. 2006; 17:634–644. [PubMed: 16314388]
22. Wang T, et al. Translating mRNAs strongly correlate to proteins in a multivariate manner and their translation ratios are phenotype specific. Nucleic Acids Res. 2013; 41:4743–4754. [PubMed: 23519614]
23. Miller PM, et al. Golgi-derived CLASP-dependent microtubules control Golgi organization and polarized trafficking in motile cells. Nat Cell Biol. 2009; 11:1069–1080. [PubMed: 19701196]
24. De Groot CO, et al. Molecular insights into mammalian end-binding protein heterodimerization. J Biol Chem. 2010; 285:5802–5814. [PubMed: 20008324]
25. Christie JM, et al. Steric interactions stabilize the signaling state of the LOV2 domain of phototropin 1. Biochemistry. 2007; 46:9310–9319. [PubMed: 17658895]

26. Ettinger A, Wittmann T. Fluorescence live cell imaging. Methods Cell Biol. 2014; 123:77–94. [PubMed: 24974023]
27. Gierke S, Wittmann T. EB1-recruited microtubule +TIP complexes coordinate protrusion dynamics during 3D epithelial remodeling. Curr Biol. 2012; 22:753–762. [PubMed: 22483942]
28. Bieling P, et al. CLIP-170 tracks growing microtubule ends by dynamically recognizing composite EB1/tubulin-binding sites. J Cell Biol. 2008; 183:1223–1233. [PubMed: 19103809]
29. Kaverina I, Straube A. Regulation of cell migration by dynamic microtubules. Semin Cell Dev Biol. 2011; 22:968–974. [PubMed: 22001384]
30. Wittmann T, Bokoch GM, Waterman-Storer CM. Regulation of leading edge microtubule and actin dynamics downstream of Rac1. J Cell Biol. 2003; 161:845–851. [PubMed: 12796474]
31. Brouhard GJ, et al. XMAP215 is a processive microtubule polymerase. Cell. 2008; 132:79–88. [PubMed: 18191222]
32. Nakamura S, et al. Dissecting the nanoscale distributions and functions of microtubule-end-binding proteins EB1 and ch-TOG in interphase HeLa cells. PLoS One. 2012; 7:e51442. [PubMed: 23251535]
33. Bouchet BP, et al. Mesenchymal Cell Invasion Requires Cooperative Regulation of Persistent Microtubule Growth by SLAIN2 and CLASP1. Dev Cell. 2016; 39:708–723. [PubMed: 27939686]
34. Etienne-Manneville S. Microtubules in cell migration. Annu Rev Cell Dev Biol. 2013; 29:471–499. [PubMed: 23875648]
35. Wittmann T, Waterman-Storer CM. Cell motility: can Rho GTPases and microtubules point the way? J Cell Sci. 2001; 114:3795–3803. [PubMed: 11719546]
36. Bouchet BP, Akhmanova A. Microtubules in 3D cell motility. J Cell Sci. 2017; 130:39–50. [PubMed: 28043967]
37. Duellberg C, et al. Reconstitution of a hierarchical +TIP interaction network controlling microtubule end tracking of dynein. Nat Cell Biol. 2014; 16:804–811. [PubMed: 24997520]
38. Usherenko S, et al. Photo-sensitive degron variants for tuning protein stability by light. BMC Syst Biol. 2014; 8:128. [PubMed: 25403319]
39. Nihongaki Y, Kawano F, Nakajima T, Sato M. Photoactivatable CRISPR-Cas9 for optogenetic genome editing. Nat Biotechnol. 2015; 33:755–760. [PubMed: 26076431]
40. Dagliyan O, et al. Engineering extrinsic disorder to control protein activity in living cells. Science. 2016; 354:1441–1444. [PubMed: 27980211]
41. Kumar A, et al. Short Linear Sequence Motif LxxPTPh Targets Diverse Proteins to Growing Microtubule Ends. Structure. 2017; 25:924–932. [PubMed: 28552577]
42. Vitre B, et al. EB1 regulates microtubule dynamics and tubulin sheet closure in vitro. Nat Cell Biol. 2008; 10:415–421. [PubMed: 18364701]
43. Maurer SP, et al. EB1 accelerates two conformational transitions important for microtubule maturation and dynamics. Curr Biol. 2014; 24:372–384. [PubMed: 24508171]
44. Duellberg C, Cade NI, Holmes D, Surrey T. The size of the EB cap determines instantaneous microtubule stability. Elife. 2016; 5
45. Stehbens SJ, et al. CLASPs link focal-adhesion-associated microtubule capture to localized exocytosis and adhesion site turnover. Nat Cell Biol. 2014; 16:558–573.
46. Mitchison TJ. The proliferation rate paradox in antimitotic chemotherapy. Mol Biol Cell. 2012; 23:1–6. [PubMed: 22210845]
47. Borowiak M, et al. Photoswitchable Inhibitors of Microtubule Dynamics Optically Control Mitosis and Cell Death. Cell. 2015; 162:403–411. [PubMed: 26165941]
48. Adikes RC, Hallett RA, Saway BF, Kuhlman B, Slep KC. Control of microtubule dynamics using an optogenetic microtubule plus end–F-actin cross-linker. J Cell Biol. 2017; 217(2):779–793. [PubMed: 29259096]
49. Akhmanova A, et al. Clasps are CLIP-115 and -170 associating proteins involved in the regional regulation of microtubule dynamics in motile fibroblasts. Cell. 2001; 104:923–935. [PubMed: 11290329]
50. Wu YI, et al. A genetically encoded photoactivatable Rac controls the motility of living cells. Nature. 2009; 461:104–108. [PubMed: 19693014]

51. Strickland D, et al. TULIPs: tunable, light-controlled interacting protein tags for cell biology. Nat Methods. 2012; 9:379–384. [PubMed: 22388287]
52. Ran FA, et al. Genome engineering using the CRISPR-Cas9 system. Nat Protoc. 2013; 8:2281–2308. [PubMed: 24157548]
53. van Haren J, Wittmann T. Generation of cell lines with light-controlled microtubule dynamics. Nat Protocol Exchange. 2017
54. Stehbens S, Pemble H, Murrow L, Wittmann T. Imaging intracellular protein dynamics by spinning disk confocal microscopy. Methods Enzymol. 2012; 504:293–313. [PubMed: 22264541]
55. Schindelin J, et al. Fiji: an open-source platform for biological-image analysis. Nat Methods. 2012; 9:676–682. [PubMed: 22743772]
56. Ettinger A, van HJ, Ribeiro SA, Wittmann T. Doublecortin Is Excluded from Growing Microtubule Ends and Recognizes the GDP-Microtubule Lattice. Curr Biol. 2016; 26:1549–1555. [PubMed: 27238282]
57. Matov A, et al. Analysis of microtubule dynamic instability using a plus-end growth marker. Nat Methods. 2010; 7:761–768. [PubMed: 20729842]
58. Jaqaman K, et al. Robust single-particle tracking in live-cell time-lapse sequences. Nat Methods. 2008; 5:695–702. [PubMed: 18641657]
59. Meijering E, Dzyubachyk O, Smal I. Methods for cell and particle tracking. Methods Enzymol. 2012; 504:183–200. [PubMed: 22264535]
60. Stehbens SJ, Wittmann T. Analysis of focal adhesion turnover: A quantitative live-cell imaging example. Methods Cell Biol. 2014; 123:335–346. [PubMed: 24974036]
61. Brown AM. A step-by-step guide to non-linear regression analysis of experimental data using a Microsoft Excel spreadsheet. Comput Methods Programs Biomed. 2001; 65:191–200. [PubMed: 11339981]

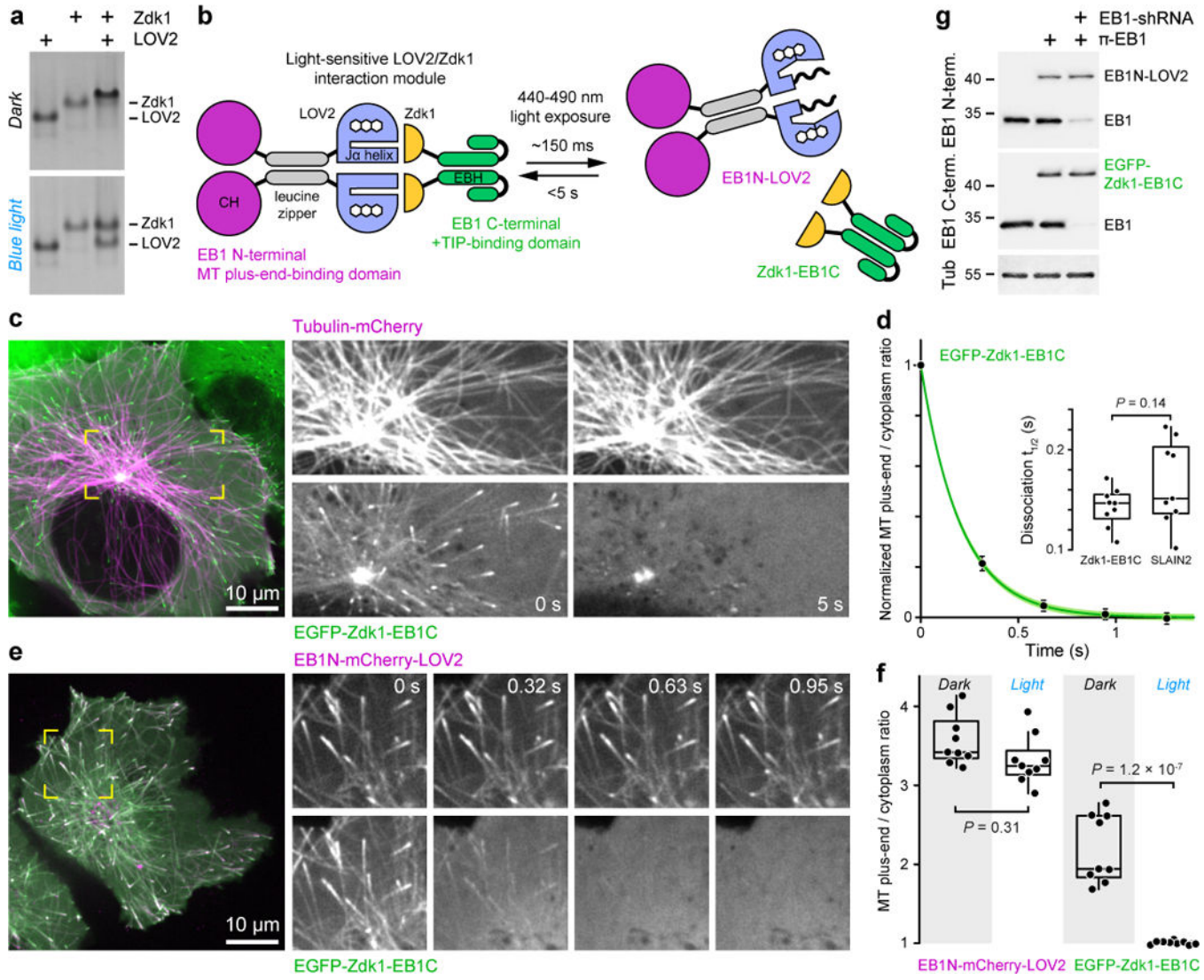

Figure 1. Design of a light-sensitive EB1 variant that can replace endogenous EB1 function

(a) Interaction of purified LOV2 and Zdk1 analysed by native PAGE. Blue light results in dissociation of the LOV2/Zdk1 complex, which is upshifted compared with the individual proteins. **(b)** Schematic of the photo-inactivated π-EB1 design resulting in reversible dissociation of the MT-binding and +TIP adapter domains upon blue light exposure. **(c)** Cell expressing tubulin-mCherry, EGFP-tagged Zdk1-EB1C and unlabelled EB1N-LOV2 before and after 5 s of 488 nm blue light exposure resulting in dissociation of Zdk1-EB1C from growing MT plus ends. **(d)** Analysis of the blue light-induced EGFP-Zdk1-EB1C dissociation rate from MT ends. Data shown are the mean +/− 95% confidence intervals of n = 9 cells. Solid line is an exponential decay fit. Inset shows comparison of dissociation half-life times of Zdk1-EB1C and SLAIN2, a +TIP that depends on EB1 for MT end association. Statistical analysis by two-tailed t-test. **(e)** Cell expressing both halves of π-EB1 fluorescently tagged showing that EB1N-LOV2 remains on growing MT ends after blue light exposure. Time stamps indicate duration of blue light exposure. Dual-wavelength images were acquired simultaneously using an emission image splitter. **(f)** Analysis of the

amount of the two π-EB1 halves bound to MT ends before and during 1 s of blue light exposure. n = 9 cells. Statistical analysis by Tukey-Kramer HSD test. **(g)** Analysis of EB1 and π-EB1 expression in H1299 cell lines in which π-EB1 constructs were stably expressed and endogenous EB1 depleted by shRNA. Immunoblots were probed with antibodies specific to either the EB1 N- or C-terminus and anti-α-tubulin as loading control. Experiments in **a** and **g** were replicated three times with similar results. Yellow boxes in **c** and **e** indicate regions shown as individual channels at higher magnification. Box plots in **d** and **f** show median, first and third quartile, with whiskers extending to observations within 1.5 times the interquartile range, and all individual data points. Unprocessed original blots in Supplementary Fig. 5. Source data in Supplementary Table 3.

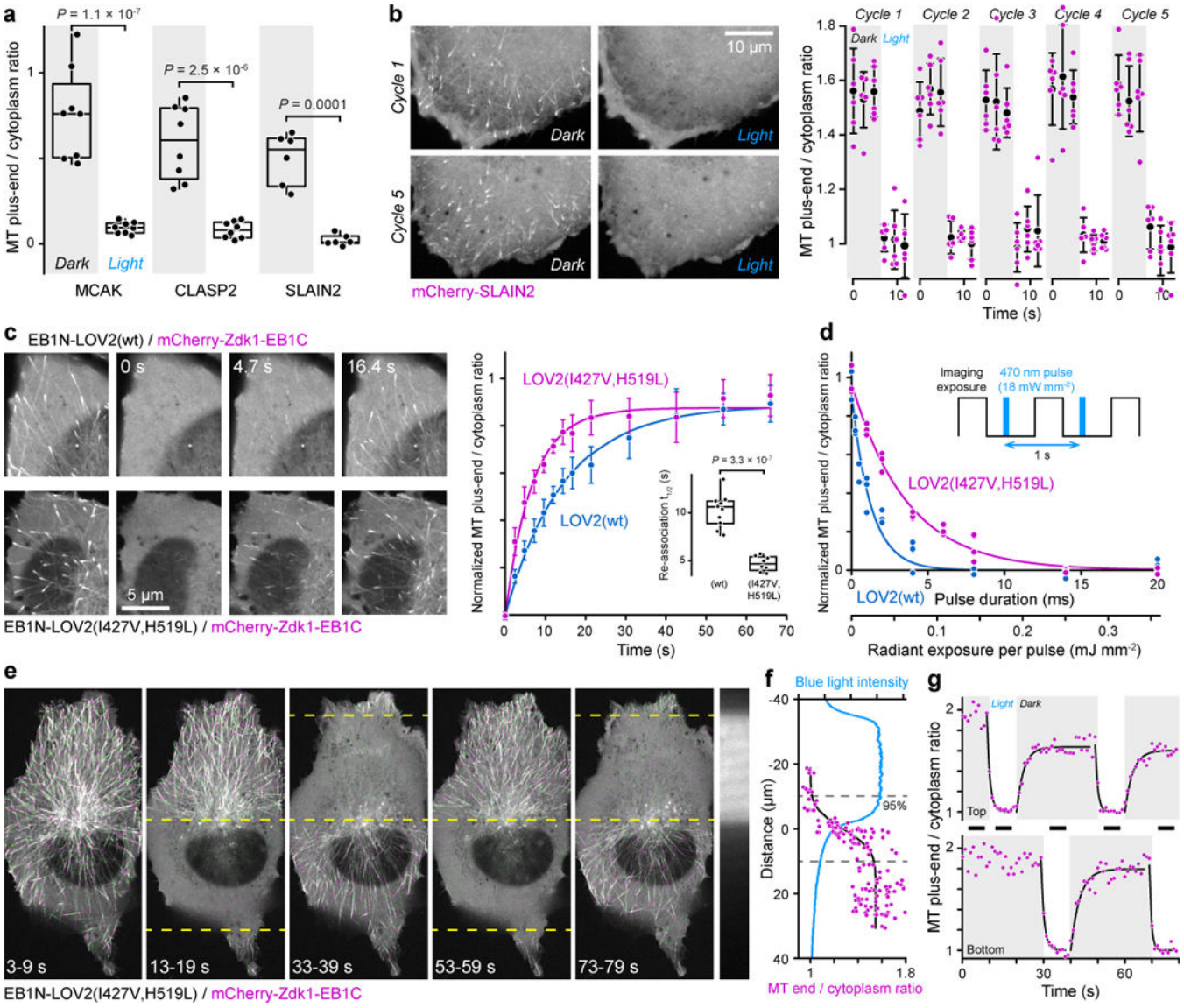

Figure 2. Spatially and temporally reversible photo-dissociation of +TIP complexes

(a) Analysis of mCherry-tagged +TIPs on MT ends before and during 1 s of blue light in π-EB1/EB1 shRNA cells. n = 8 (MCAK, CLASP2) and 6 cells (SLAIN2). Statistical analysis by Tukey-Kramer HSD test. **(b)** Reversible blue light-induced mCherry-SLAIN2 dissociation from MT ends in π-EB1/EB1 shRNA cells. Graph shows the mean +/− standard deviation and individual measurements from the cell shown over multiple blue light cycles. **(c)** Comparison of Zdk1-EB1C recovery on MT plus ends in cells expressing π-EB1 containing the indicated LOV2 variant. Graph compares Zdk1-EB1C re-association with LOV2(wt) (n = 10 cells) or LOV2(I427V,H519L) (n = 8) showing the mean +/− 95% confidence intervals. Solid lines are exponential curve fits. Statistical analysis by two-tailed t-test. **(d)** Zdk1-EB1C MT plus-end-association in π-EB1 constructs with the indicated LOV2 variants as function of radiant exposure at steady state after 40 s of pulsed blue light. Exposure was varied by pulse width modulation. Solid lines are exponential curve fits. **(e)** Patterned blue light exposure within the regions indicated by dashed lines shows high

spatiotemporal accuracy of π-EB1 photo-dissociation. The light pattern is switched every 10 s. Images are projections of the indicated time periods (black bars in **g**) showing sequential time points in alternating green and purple. Right panel: top blue light pattern reflected off the cover glass. **(f)** Zdk1-EB1C MT plus-end-association at the boundary of the blue light pattern corresponding to the 33-39 s period. Dashed lines demarcate the 95% switch (i.e. +/− 2 σ) in MT end association calculated from a cumulative normal distribution fit (black line). The intensity profile of the light pattern (blue line) was measured from the pattern image in **e**. **(g)** Zdk1-EB1C MT plus-end-association as function of time in the top and bottom halves of the cell in **e**. Solid lines are exponential curve fits. Shaded areas indicate time periods without blue light exposure. Box plots in **a** and **c** show median, first and third quartile, with whiskers extending to observations within 1.5 times the interquartile range, and all individual data points. Source data in Supplementary Table 3.

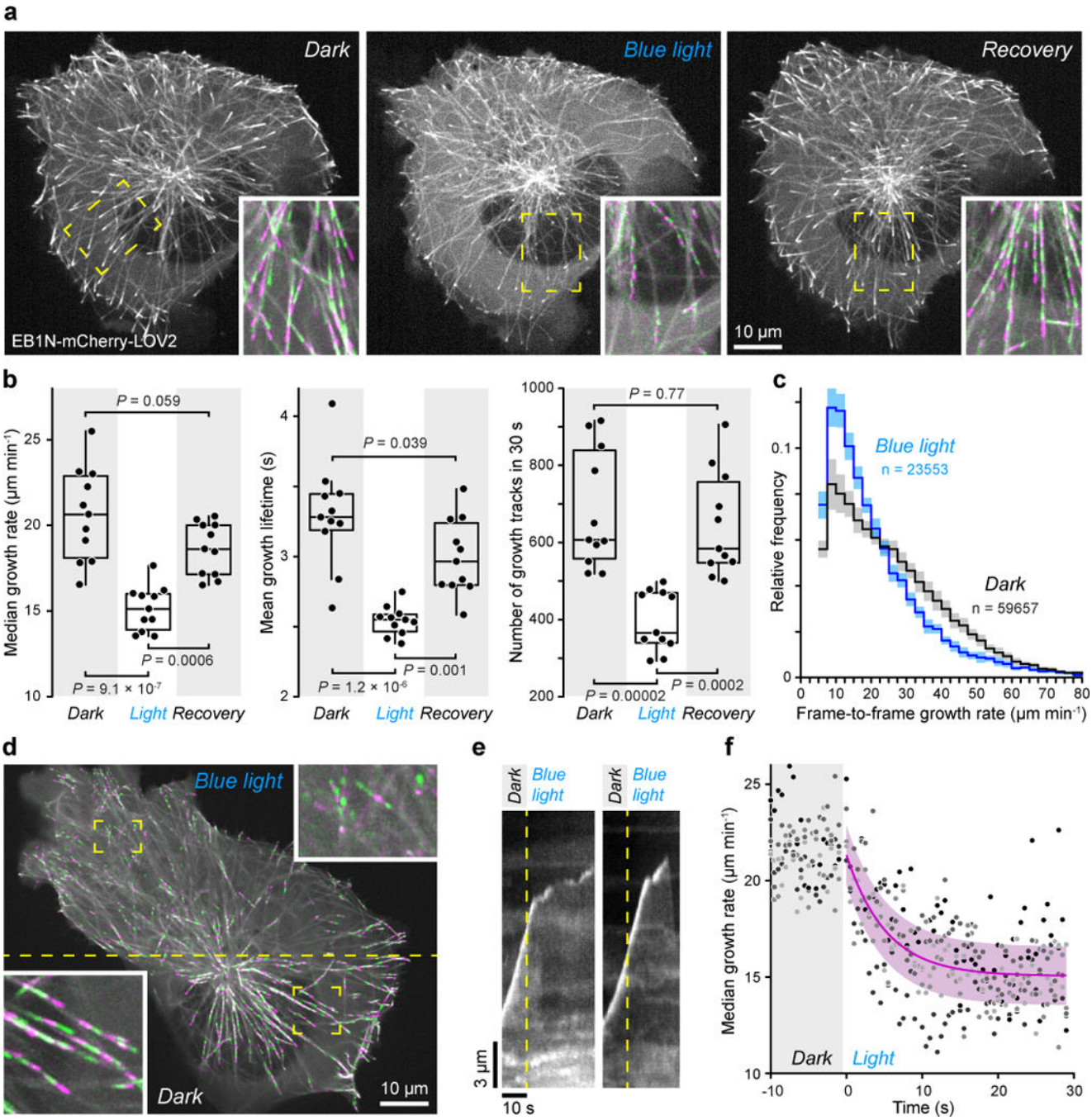

Figure 3. Attenuation of MT growth by π-EB1 photo-dissociation

(a) EB1N-mCherry-LOV2 labelled MT plus ends before, after 30 s during blue light exposure, and after 3 min recovery in the dark in π-EB1/EB1 shRNA cells. Insets show maximum intensity projections over 20 s time windows of the indicated regions at higher magnification. MT growth tracks appear in alternating colours. **(b)** Quantification of MT polymerization dynamics by tracking EB1N-mCherry-LOV2 labelled MT ends. Growth rates are frame-to-frame measurements from images acquired at 0.5 s intervals. n = 11 cells. Box plots show median, first and third quartile, with whiskers extending to observations

within 1.5 times the interquartile range, and all individual data points. Statistical analysis by Tukey-Kramer HSD test. **(c)** Comparison of the frame-to-frame MT growth rate distribution in the dark and during blue light exposure demonstrating a specific loss of fast growth events as a result of π-EB1 photo-dissociation. Shown are the mean distributions from the cells in **b** (lines) and 95% confidence intervals (shaded areas). **(d)** Local inhibition of MT growth by patterned blue light exposure in a π-EB1/EB1 shRNA cell expressing EB1N-mCherry-LOV2. Shown is a maximum intensity projection over 20 s. MT growth tracks appear in alternating colours. Only the top half above the dashed line was exposed to blue light pulses between image acquisitions. Insets show the indicated regions at higher magnification. This experiment was replicated more than five times with similar results. **(e)** Representative kymographs illustrating the sudden response of rapidly growing MT ends to π-EB1 photo-dissociation. **(f)** Analysis of the intracellular MT population growth rate response as a function of time after π-EB1 photo-dissociation. Shown are all measurements from n = 5 cells. Solid line is an exponential fit of the mean during blue light exposure. Shaded area is the 95% confidence interval of the fit. Source data in Supplementary Table 3.

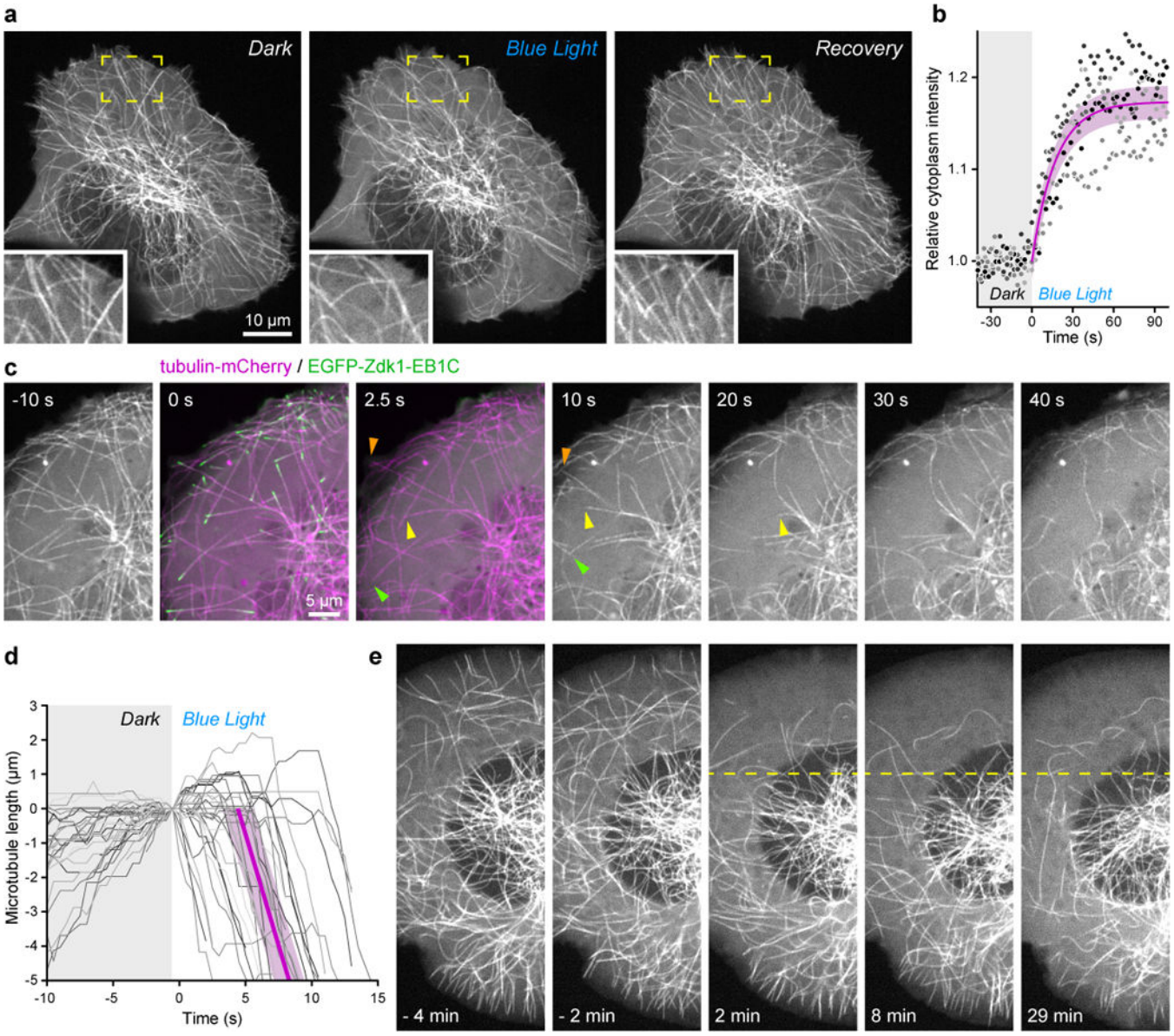

Figure 4. π-EB1 photo-dissociation induced MT cytoskeleton reorganization

(a) Tubulin-mCherry expressing π-EB1/EB1 shRNA cell before, after 30 s during blue light exposure, and after 3 min recovery in the dark. Insets show the indicated regions at higher magnification demonstrating reversible decrease of MT density near the cell periphery. **(b)** Analysis of the relative amount of cytoplasmic tubulin-mCherry in response to π-EB1 photo-dissociation. Shown are all measurements from n = 5 cells normalized to the dark condition. Solid line is an exponential fit of the mean during blue light exposure. Shaded area is the 95% confidence interval of the fit. **(c)** Rapid depolymerisation of MTs in the cell periphery in response to π-EB1 photo-dissociation. Arrows highlight example MTs. **(d)** Life-history plots of MTs with ends near the cell edge aligned to the time of blue light exposure. n = 33 MTs from 5 cells. The purple line is the average of linear fits of the depolymerizing phase of these MTs. Shaded area indicates 95% confidence interval. **(e)**

Time-lapse sequence of tubulin-mCherry in a Rac(Q61L)-expressing π-EB1 cell in response to local blue light exposure (above the dashed line) illustrating sustained reorganization of the MT network. This experiment was replicated more than five times with similar results. Source data in Supplementary Table 3.

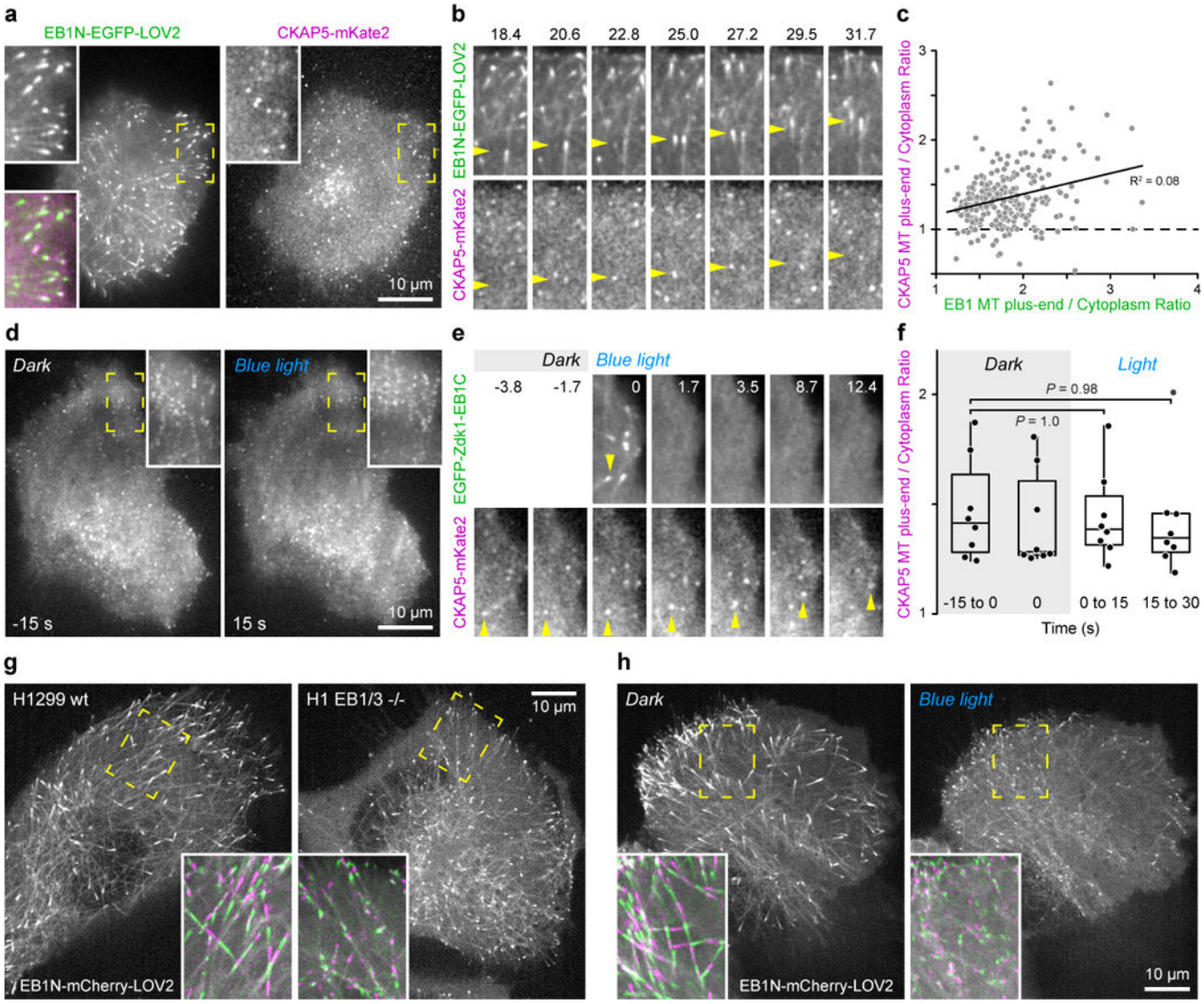

Figure 5. EB1-independent MT plus end localization of the MT polymerase CKAP5

(a) TIRF microscopy of a control H1299 cell expressing EB1N-EGFP-LOV2 and CKAP5-mKate2. Note that wavelengths were acquired sequentially resulting in a small temporal shift between channels, and punctate appearance of CKAP5 compared to the typical comet shaped EB1 distribution. Insets show indicated regions at higher magnification. **(b)** Time-lapse sequence showing variable and transient CKAP5 accumulation on MT ends. Arrows highlight representative MT ends. Elapsed time in seconds. **(c)** Scatter plot of the relative accumulation of CKAP5 and EB1 on the same MT ends showing only a very weak correlation. Solid line is a linear fit. n = 252 MT ends from 5 cells. **(d)** TIRF microscopy of CKAP5-mKate2 in a π-EB1/EB1 shRNA cell 15 s before and during π-EB1 photo-dissociation showing qualitative indistinguishable CKAP5 distribution. Insets show projections over 20 s time windows of the indicated regions, revealing linear tracks of CKAP5 dots. **(e)** Time-lapse sequence of CKAP5-mKate2 dynamics before and during blue light exposure in a π-EB1/EB1 shRNA cell. Arrows highlight linear movement of MT end-

associated CKAP5 dot. Elapsed time in seconds. **(f)** CKAP5 enrichment on MT ends in the indicated time intervals before and during blue light exposure indicating no change in response to π-EB1 photo-dissociation. Statistical analysis by Tukey-Kramer HSD test. Box plots show median, first and third quartile, with whiskers extending to observations within 1.5 times the interquartile range, and all individual data points. n = 8 cells. **(g)** EB1N-mCherry-LOV2 labelled MT plus ends in control H1299 cells and in cells in which both EB1 and EB3 expression were deleted by CRISPR/Cas9 genome editing showing attenuation of MT growth in EB1/3 −/− cells. **(h)** EB1N-mCherry-LOV2 labelled MT plus ends in a EB1/3 −/− π-EB1 rescue cell before and during blue light exposure demonstrating light-induced MT growth attenuation very similar to what we observe in π-EB1/EB1 shRNA cells. In **g** and **h**, insets show maximum intensity projections over 20 s time windows of the indicated regions. MT growth tracks appear in alternating colours. Experiments were replicated more than five times with similar results. Source data in Supplementary Table 3.

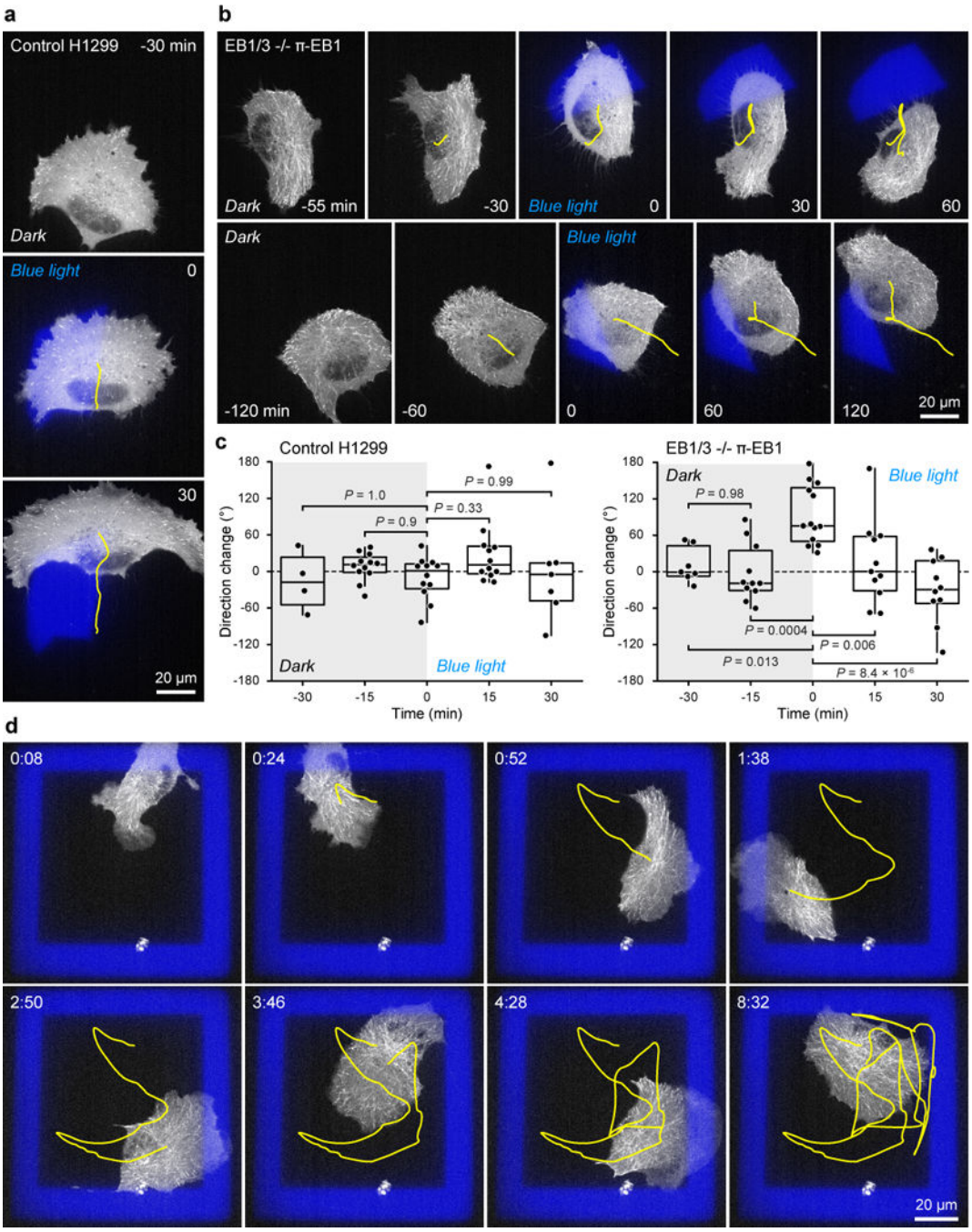

Figure 6. Aversive cell turning in response to local π-EB1 photo-dissociation

(a) Time-lapse sequence of a control H1299 cell expressing EB3-mCherry showing no response to local blue light exposure. **(b)** Two examples of EB1/3 −/− π-EB1 rescue cells that turn away from local blue light exposure in the front half of the cell. Cells also express mCherry-Zdk1-EB1C to show local π-EB1 photo-dissociation. Blue areas are images of the blue light exposure patterns reflected off the coverslip. Yellow lines show the cell centroid trajectory. 0 min indicates the time when the respective blue light pattern was switched on. **(c)** Analysis of cell migration direction changes over half hour time intervals expressed as

the angle between smoothened centroid positions 15 min before and 15 min after the indicated time points. A significant non-random change in migration direction only occurred in response to local blue light exposure in EB1/3 −/− π-EB1 rescue cells, which consistently turned away from the pattern. n = 12 cells (control); 13 cells (EB1/3 −/− π-EB1). Box plots show median, first and third quartile, with whiskers extending to observations within 1.5 times the interquartile range, and all individual data points. Statistical analysis by Tukey-Kramer HSD test. **(d)** Time-lapse sequence of a migrating EB1/3 −/− π-EB1 rescue cell trapped inside a virtual blue light box for over 8 hours. Yellow line marks the centroid trajectory. This was replicated more than three times with similar results.